

# A process-based, spatially-distributed model for streambank erosion rate

Mitchell McMillan\*, Zhiyong Hu

*The University of West Florida, Department of Earth and Environmental Sciences,  
Pensacola, FL*

---

## Abstract

Streambank erosion is a major source of fluvial sediment and has been identified as a cause of sediment pollution, but few large-scale spatially distributed models to quantify streambank erosion rates exist. We introduce a spatially distributed model for streambank erosion that can be readily applied in watersheds throughout the globe. The model is based on the familiar excess-velocity equation and is comprised of 3 components: a physics-based hydrodynamic model, a watershed hydrology model, and a bank erodibility parameterization. The hydrodynamic submodel requires channel centerline, drainage area, and Manning's roughness as data inputs; the hydrological submodel utilizes the Noah land surface model with North American Land Data Assimilation Systems Phase 2 (NLDAS-2) monthly forcings to estimate monthly average discharge and flow depth via Manning's equation; bank erodibility is based on tree cover and bank height as proxies for root density. The streambank erosion model was calibrated with erosion rates measured

---

\*Corresponding author

Email addresses: [mcmillan@students.uwf.edu](mailto:mcmillan@students.uwf.edu) (Mitchell McMillan), [zhu@uwf.edu](mailto:zhu@uwf.edu) (Zhiyong Hu)

throughout the northern Gulf of Mexico coastal plain. Despite several extreme precipitation events occurring during the study period, the calibrated model predicted streambank erosion rates with a Pearson's correlation coefficient  $R = 0.55$  and only 3 free parameters. An example of reach-scale model application is illustrated on  $\sim 1$  km of a medium-sized, mixed forest-pasture stream, where non-forested meander bends are estimated to erode up to 0.75 m/yr, while forested bends are estimated to rarely exceed 0.25 m/yr. Spatially-distributed, process-based modelling of streambank erosion rates has broad implications for the stream restoration and landscape modelling communities.

*Keywords:* Geographic Information Systems; Root distribution;  
Meandering streams; Hydraulic modelling

---

## **1. Introduction**

Streambank erosion is one of the most visible ways that rivers adjust to changes in discharge, sediment supply, and floodplain composition (Leopold and Wolman, 1960). Outer bank erosion, along with inner bank accretion, is responsible for meander migration and the long-term evolution of river channel planforms (Crosato, 2009; Eke et al., 2014; Parker et al., 2011). Not only a key physical process, bank erosion creates and maintains diverse riparian habitats, supplies river channels with large woody material (Florsheim et al., 2008), and is a major source of fluvial sediment (Bull, 1997; Kronvang et al., 2013; Sekely et al., 2002). Over the last few decades, it has become clear that accelerated bank erosion is often a signature of human impacts such as channelization (Hupp and Simon, 1991), agriculture (Kemp et al., 2016; Knox,

13 2006; Walter and Merritts, 2008), and the pervasive construction and demise  
14 of milldams (Lyons et al., 2015; Merritts et al., 2011; Pizzuto, 2009). In the  
15 U.S., streambank erosion is a major nonpoint source of sediment pollution  
16 (U.S. Environmental Protection Agency, 2000). As fluvial systems adjust to  
17 increasing human influences (Gregory, 2006), it is important to understand  
18 how rates of streambank erosion may respond to changes in land use/land  
19 cover, runoff, and other climate variables (Pelletier et al., 2015).

20 Previous studies have investigated the processes that control rates of bank  
21 erosion, including weathering, fluvial erosion, and mass wasting. Flow around  
22 meander bends results in the development of a helical secondary flow, directed  
23 inward near the channel bed (Leopold and Wolman, 1960), that produces  
24 characteristic bed geometry patterns of shallow point bars and deep pools  
25 (Hooke, 1975). The modified bed geometry shifts the primary flow toward  
26 the deeper portions of the channel and the outer banks of meander bends  
27 (Dietrich et al., 1979; Dietrich and Smith, 1983; Hooke, 1975). These two  
28 processes increase the shear stresses acting on the bank, which leads to basal  
29 scour and bank steepening. With continued steepening, geotechnical insta-  
30 bility and eventually bank failure occur (Lawler et al., 1997; Thorne, 1982),  
31 possibly followed by slump block armoring (Parker et al., 2011). Failure is re-  
32 sisted by effective cohesion, matric suction, and mechanical reinforcement by  
33 vegetation roots (Osman and Thorne, 1988; Pollen, 2007; Pollen and Simon,  
34 2005; Simon et al., 2000; Thomas and Pollen-Bankhead, 2010).

35 Although near-bank shear stress is forced by channel curvature variations,  
36 the flow does not instantaneously adapt to these variations; a spatial lag de-  
37 velops between maximum curvature and maximum shear stress (Crosato,

38 2009). The spatial lag distance is proportional to  $C_f^{-1}H$  (the product of  
39 channel roughness and flow depth) (Blanckaert and de Vriend, 2010), and  
40 can be dramatically decreased by vegetation and vegetation-induced bank  
41 irregularities (Thorne and Furbish, 1995), further reinforcing the fundamen-  
42 tal importance of bank vegetation in the spatial and temporal evolution of  
43 streambanks.

44 Below-ground root distributions remain difficult to quantify, but obser-  
45 vations have shown that streambank erosion rates are often sensitive to  
46 biomass density (Micheli and Kirchner, 2002; Perucca et al., 2007), root  
47 density (Micheli and Kirchner, 2002; Wynn and Mostaghimi, 2006), forest  
48 cover (Allmendinger et al., 2005; Hubble et al., 2010; Micheli et al., 2004;  
49 Stott, 1997), tree density (Konsoer et al., 2016; Pizzuto and Meckelnburg,  
50 1989; Sass and Keane, 2012), and soil properties such as texture and bulk  
51 density (Couper, 2003; Julian and Torres, 2006; Konsoer et al., 2016; Piz-  
52 zuto, 1984; Wynn and Mostaghimi, 2006). On the other hand, recent work  
53 on bank erodibility using jet erosion tests suggests that site-specific (rather  
54 than watershed-scale) relationships must be derived from soil properties to  
55 estimate bank erodibility parameters (Daly et al., 2015). This suggests that  
56 while a purely mechanical model of bank failure is likely to require intensive  
57 collection of local data, geospatial data such as tree cover may be used as a  
58 proxy for some important aspects of bank erodibility such as root reinforce-  
59 ment. Bank erosion rates have also shown a correlation with drainage area;  
60 this has been explained by a downstream increase in bank height (and thus  
61 instability) (Hooke, 1980) or by stream power, which peaks in the middle  
62 portions of large drainage basins (Lawler et al., 1999).

63 For cohesive sediments, fluvial erosion is often modeled as proportional to  
64 the magnitude of near-bank shear stress above some critical value (Parthe-  
65 niades, 1965). Existing models of streambank erosion have quantified near-  
66 bank shear stress in a variety of ways. Following the work of Ikeda et al.  
67 (1981), a hierarchy of coupled hydrodynamic-morphodynamic models has  
68 been developed based on the assumption that bank erosion rate  $\zeta$  (m/s) is  
69 proportional to the excess near-bank velocity,

$$\zeta = E\Delta U \quad (1)$$

70 where  $\Delta U$  (m/s) is the near-bank excess velocity (near-bank velocity  $u_b$  minus  
71 bulk velocity  $U_s$ ), and  $E$  is a dimensionless calibration coefficient often called  
72 the bank erodibility coefficient (Camporeale et al., 2007). Although it is  
73 sometimes assumed that the so-called erodibility coefficient depends only  
74 on soil and vegetation properties, it also accounts for numerical constants  
75 related to the implementation of a given hydrodynamic model (Mosselman,  
76 2014) as well as any processes of opposite-bank accretion that also drive  
77 meander migration (Crosato, 2009). The excess velocity relationship can  
78 be thought of as a linearized form of the excess shear stress equation, and  
79 has been tentatively confirmed by field observations (Odgaard, 1987, 1989;  
80 Pizzuto and Meckelnburg, 1989) and long-term simulations of natural river  
81 reaches (Matsubara and Howard, 2014). Equation (1) is an example of a  
82 geomorphic transport law (Dietrich et al., 2003).

83 Models are already available for quantifying soil erosion and transport  
84 from drainage basins, but they lack a bank erosion component (de Vente  
85 et al., 2013). The applied community (e.g., stream restoration practitioners)  
86 employ field-based, empirical models such as Rosgen's BANCS to estimate

87 bank erosion rates (Rosgen, 2001, 2009; Simon and Doyle, 2007), but re-  
88 searchers attempting to calibrate such models have reported mixed results  
89 (Harmel et al., 1999; Kwan and Swanson, 2014; McMillan, 2016; Sass and  
90 Keane, 2012; Van Eps et al., 2004). Heavy reliance on visual estimates (e.g.,  
91 of root density), the need for extensive field data collection, and the lack  
92 of a process-based near-bank shear stress model diminish the utility of this  
93 approach. A recent attempt to extend the BANCS approach with aerial im-  
94 agery and GIS data demonstrated the need for a spatially distributed bank  
95 erosion model, but itself was limited by its empirical, semi-quantitative ap-  
96 proach (Bandyopadhyay et al., 2014). While it is impractical to directly  
97 simulate all of the processes responsible for erosion at every streambank, a  
98 combination of physics-based modelling with empirical calibration can yield  
99 powerful predictive tools (Pelletier, 2012, e.g.).

100 **2. Model concepts and overview**

101 The model of this paper quantifies annual streambank erosion rates by  
102 employing three interacting submodels: (1) a large-scale, 1-dimensional flow  
103 model of monthly discharge (hydrological submodel), (2) a physics-based hy-  
104 drodynamic flow model (hydrodynamic submodel), and (3) a model of bank  
105 erodibility based on tree cover and bank height (bank erodibility submodel).  
106 Figure 1 gives a high-level overview of these components, their data require-  
107 ments, and how they fit into the conceptual model (transport law) for bank  
108 erosion.

109 Streambank erosion rate  $\hat{\zeta}$  was modeled as

$$\hat{\zeta} = E\overline{\Delta U} \quad (2)$$

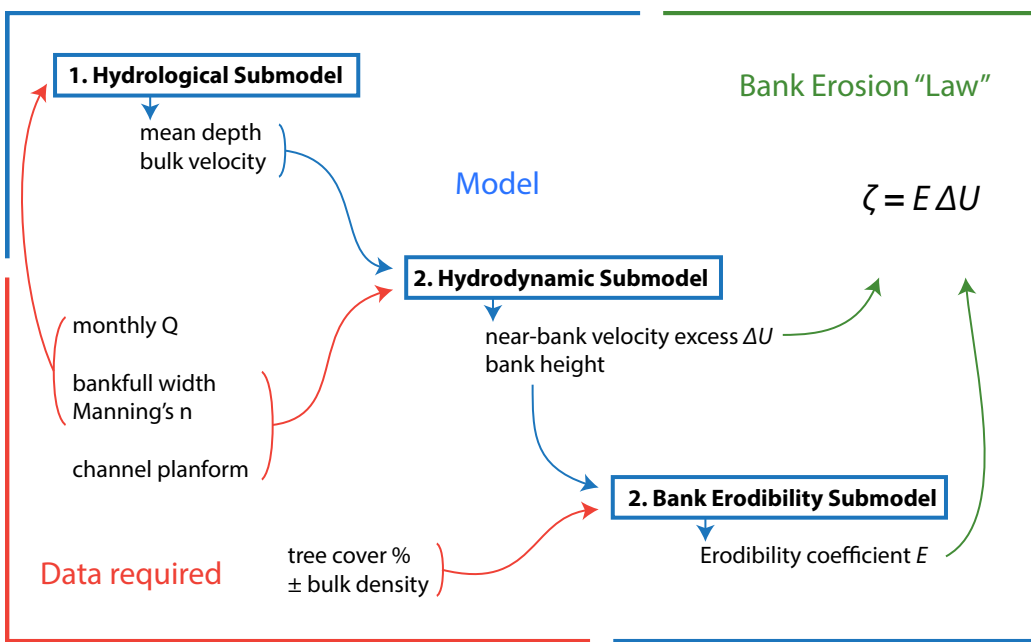


Figure 1: Illustration of model data requirements, 3 main components, and the geomorphic transport law used to model streambank erosion rate  $\zeta$ .

110 where  $E$  is bank erodibility and  $\overline{\Delta U}$  is the average near-bank velocity excess  
 111 for a given simulation period. For model calibration, simulation periods  
 112 ranged from 22 to 24 months for each location, depending on the dates of  
 113 erosion rate measurements.

114 The bank erodibility coefficient  $E$  was assumed to be proportional to  
 115 soil erodibility  $K$ . Two representations of soil erodibility,  $K_1$  and  $K_2$ , were  
 116 investigated. Wynn and Mostaghimi (2006) provided an empirical equation  
 117 for sandy streambank soils in southwestern Virginia expressed as a function  
 118 of coarse root density  $RD$  and soil bulk density  $BD$ ,

$$K_1 = c_0 \exp(c_1 \ln RD - c_2 BD^{2.5}). \quad (3)$$

119 which constitutes the first representation of soil erodibility. Due to the nor-  
 120 malization and empirical fitting of the original data by Wynn and Mostaghimi  
 121 (2006), we replaced the coefficients with generic free parameters denoted by  
 122  $c$ ; the exponent of 2.5 was retained. Pizzuto (1984) and Pizzuto and Meck-  
 123 elnburg (1989) found that for forested streambanks, bank erodibility was not  
 124 related to soil properties but was largely controlled by vegetation density.  
 125 Therefore, the second representation of soil erodibility was a power function  
 126 of root density,

$$K_2 = c_0 RD^{c_1}. \quad (4)$$

127 In both  $K_1$  and  $K_2$ , root density  $RD$  was estimated as a function of tree cover  
 128 (Allmendinger et al., 2005) and bank height. Because root distributions  
 129 decrease exponentially with depth below the ground surface (Zeng, 2001),  
 130  $RD$  was modeled as

$$RD = c_0 TC^{c_1} \exp(c_2 H_b) \quad (5)$$

131 where  $TC$  is tree cover percentage,  $H_b$  is bank height (m), and the various  
132 free parameters  $c$  have been combined as appropriate. The model contains  
133 4 free parameters with  $E = K_1$  or 3 free parameters with  $E = K_2$ . The  
134 following sections detail the implementation of this model and present the  
135 results of calibrating the model using streambank erosion rates measured  
136 over a period of 2.5 years in the northern Gulf of Mexico coastal plain.

### 137 **3. Data sources and processing**

#### 138 *3.1. Streambank erosion calibration database*

139 Streambank erosion rates were measured during the 2014, 2015, and 2016  
140 water-years at 30 streambank locations throughout the northern Gulf of Mex-  
141 ico coastal plain (Figure 2). The study locations were selected to represent  
142 variability in channel size, geometry, and vegetation density. Streambank  
143 erosion was monitored using repeated cross-profiling (Lawler, 1993), result-  
144 ing in streambank erosion rates averaged over two years for each location.  
145 Erosion rates ranged from zero to over 1.3 m/yr and were heavily right-  
146 skewed. These erosion rates were used to calibrate the model; because the  
147 model was designed to utilize widely available remote sensing data rather  
148 than field data collection, no other field measurements were incorporated  
149 into model. Because this paper models erosion processes and not deposition,  
150 locations that had negative erosion rates ( $n = 4$ ) were assigned values of zero  
151 and included in the modelling.

#### 152 *3.2. Channel geometry data*

153 Table 1 summarizes the model input data. Bankfull channel width  $B$  and  
154 bankfull mean depth  $H_0$  were estimated using regional curves developed by

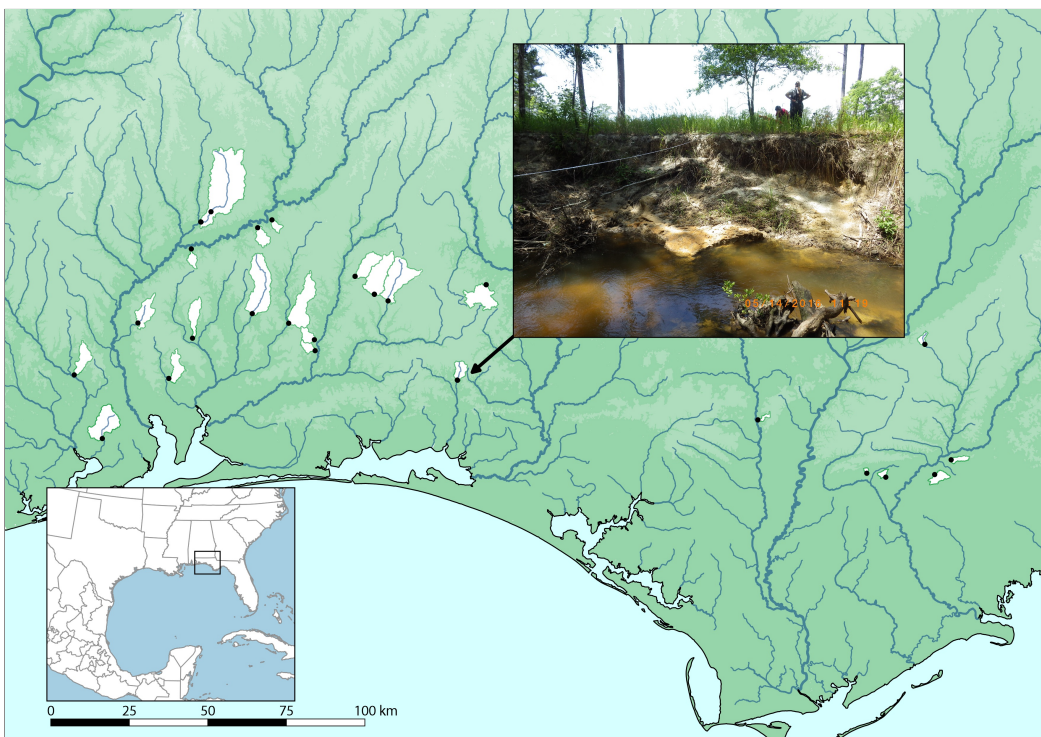


Figure 2: Topographic map showing locations of measured streambank erosion rates (black circles) and their corresponding watershed areas (white). Inset map: Location of the study area within the northern Gulf of Mexico coastal plain. Photograph: Sconnier's Mill Creek bank erosion measurement location.

Model input	Data source	Note
<i>Monthly time series</i>		
Flow depth $H$	Manning's equation	Steady, uniform flow
Event discharge $Q^*$	Noah-2.8 LSM	See Table 3
<i>Time-constant</i>		
Width $B$	Regional curves	Function of drainage area
Friction factor $C_{f,0}$	Manning's $n = 0.087$	See Table 2
Curvature $R^{-1}$	Digitized on DEM	PCS-interpolated
Longitudinal slope $S$	Extracted from DEM	Robust linear fitting
Scour factor $A$	Assumed to be 3	Default value
Tree cover $TC$	GLCF	See Table 3
Bulk density $BD$	SSURGO	See Table 3

Table 1: Sources of data inputs for the streambank erosion model

155 Metcalf et al. (2009). Regional curves predict bankfull channel geometry from  
156 drainage area. Similar equations are available in many regions of the United  
157 States (Bieger et al., 2015; Faustini et al., 2009). In the U.S., the Natural Re-  
158 sources Conservation Service maintains a database of regional curve studies  
159 organized by physiographic province (NRCS, Regional Hydraulic Geometry  
160 Curves, [http://www.nrcs.usda.gov/wps/portal/nrcs/detail/national/water/?cid=nrcs143\\_015052](http://www.nrcs.usda.gov/wps/portal/nrcs/detail/national/water/?cid=nrcs143_015052)). If regional curves are unavailable, channel geometry  
161 can be estimated with other methods or measured in the field. For a given  
162 reach,  $B$  was held constant throughout all model simulations and  $H_0$  was  
163 only used to set the initial bed geometry. Spatial and temporal variation in  
164 flow depth were modeled explicitly (Section 3.6).

166 Drainage areas were extracted from the National Hydrography Dataset  
167 (NHD) Plus v2 using the NHD Plus v2 Basin Delineator Tool. Due to heavy  
168 tree cover, channel centerlines were digitized on USGS 3D Elevation Pro-  
169 gram (3DEP) DEM (horizontal resolution 1 to 3 m (<http://nationalmap.gov/3DEP/>)). In less heavily-forested areas, channel centerlines can be accu-  
170 rately digitized using aerial or satellite imagery (Güneralp et al., 2013, 2014;  
171 Güneralp and Rhoads, 2007).

173 Digitized centerlines were interpolated with parametric piecewise-cubic  
174 spline (PCS) functions  $X(s)$  and  $Y(s)$ , where  $s$  is downstream distance, and  
175 curvature was calculated analytically as

$$\frac{1}{R} = \frac{X'Y'' - Y'X''}{[(X')^2 + (Y')^2]^{3/2}} \quad (6)$$

176 where  $R$  is radius of curvature (Güneralp and Rhoads, 2007). The down-  
177 stream coordinate  $s$ , curvature  $1/R$ , and unit normal vectors  $n$  were dis-  
178 cretized at intervals of  $B/10$ . Figure 3 plots these interpolated channel cen-

terlines, which were ultimately used to train the model. Channel gradients were estimated by extracting a topographic profile along the channel centerline and robust weighted linear regression fitting. For some reaches that were not resolved by the 3DEP DEM due to especially dense vegetation cover, a 50 cm DEM was created from terrestrial laser scanning (TLS) data collected during the study period. TLS DEMs were obtained data by taking the minimum height of each 50 cm grid cell (Figure 4).

### 3.3. Monthly streamflow data

The Noah-2.8 land surface model (LSM) with National Land Data Assimilation Systems Phase 2 (NLDAS-2) forcings (Mitchell et al., 2004; Xia et al., 2012) allowed calculation of the average monthly discharge from each drainage basin  $Q_m$ . These data are available in  $1/8^\circ$  grid cells representing average values within each cell. This scale is similar in size to many of the watersheds in this study. Due to the coarse resolution, a pre-processing step was applied of cubic convolution downscaling to  $\sim 100$  m.  $Q_m$  was computed as the sum of basin-accumulated baseflow and surface runoff during each month.

Streamflow was simulated for each month by assuming a monthly event discharge, i.e., the average discharge through the channel during periods of high flow events. Event discharge is more relevant for bank erosion than average monthly or average annual discharge, which tend to be significantly lower due to long periods of baseflow. A simple method was devised to quantify the event discharge  $Q_m^*$  for each month  $m$  as  $Q_m^* = Q_m/f_m$ , where  $Q_m$  is average monthly discharge, and  $f_m$  is monthly storm frequency. Average monthly storm frequency was calculated from daily gridded precipitation

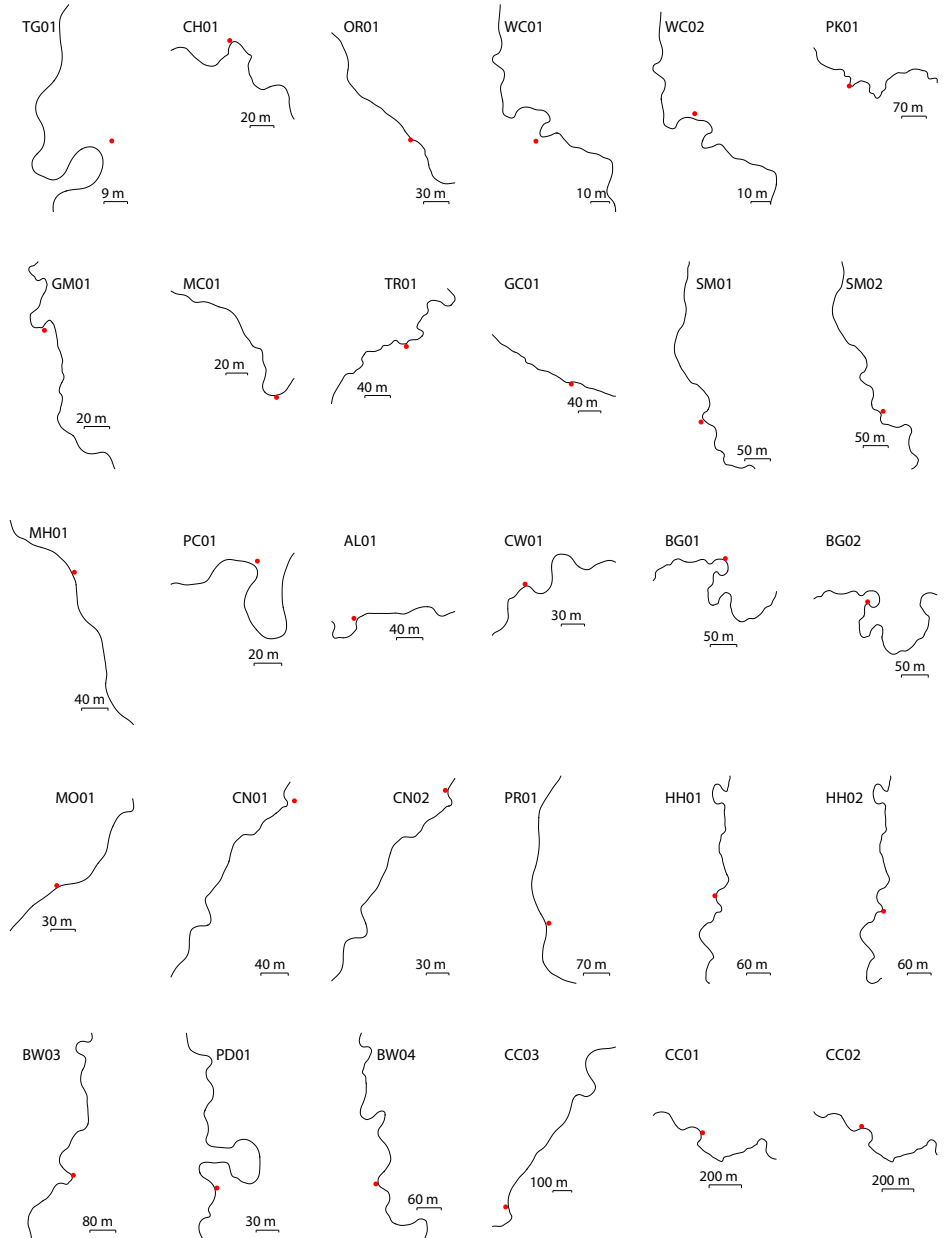


Figure 3: Illustration of channel centerlines derived from piecewise-cubic spline interpolation. Red dots show the locations of streambank erosion monitoring sites.

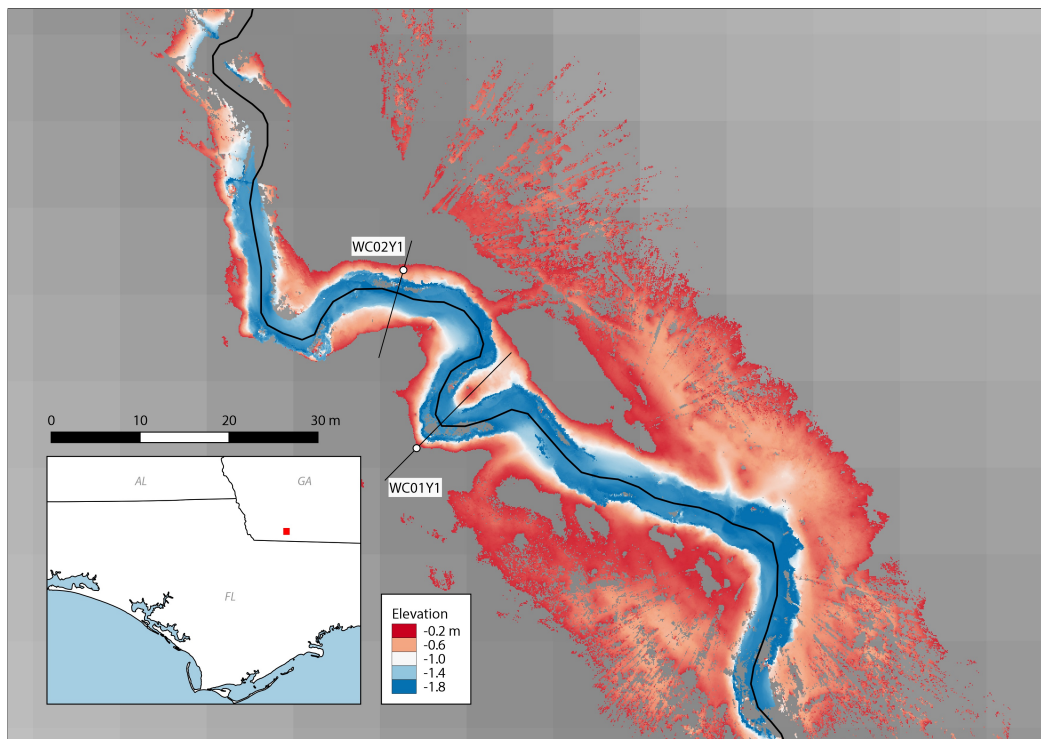


Figure 4: Example DEM created from TLS data collected during the study period overlaid on a DEM of the highest-available resolution at the time of writing (10 m National Elevation Dataset) showing two streambank erosion monitoring sites (WC01, WC02) and the digitized channel centerline (gray polyline). Willacoochee Creek, Georgia.

204 rasters from the PRISM Climate Group ([www.prismclimate.org](http://www.prismclimate.org)) as the  
 205 ratio of wet days (>1 mm precipitation) to total days in each month (Rossi  
 206 et al., 2016). Note that as storm frequency approaches 1,  $Q_m^*$  approaches  
 207 the average monthly discharge, and as storm frequency decreases toward 0,  
 208  $Q_m^*$  increases relative to  $Q$ . This reflects the strong effects that large, in-  
 209 frequent storms may have on streamflow.  $Q_m^*$  was assigned to 0 for months  
 210 with  $f_m = 0$ , though this did not occur during the study period.

211 *3.4. Channel friction*

212 Dimensionless channel friction is defined as the square of the shear veloc-  
 213 ity divided by average velocity,

$$C_f = \left( \frac{u_*}{U_s} \right)^2 \quad (7)$$

214 where  $u_* = \sqrt{\tau/\rho}$  is the shear velocity,  $\tau$  is average boundary shear stress,  
 215 and  $\rho$  is the density of water. The hydrodynamic model described below  
 216 requires the dimensionless friction factor for a theoretical straight channel,  
 217  $C_{f,0}$ , and the extra drag induced by meandering is simulated by the hydrody-  
 218 namic model itself. Therefore, Equation (7) is written in terms of Manning's  
 219  $n$ ,

$$C_{f,0} = \frac{gR_h S}{U_s^2} = g \left( \frac{n}{R_h^{1/6}} \right)^2 \quad (8)$$

220 which allows straight channel roughness to be calculated by assuming a con-  
 221 stant  $n$ . The values given in Table 2 correspond to  $C_{f,0}$  values around 0.05  
 222 to 0.11, which are significantly larger than the values for rivers reported by  
 223 (Ottevanger et al., 2012), but representative of the sharp, narrow, highly  
 224 vegetated channels in the study area (Thorne and Furbish, 1995).

Component	Modeled value	Meaning
$n_b$	0.012	Sand bed with $D_{50} \sim 0.2$ mm
$n_1$	0.01	Moderate–severe surface irregularity
$n_2$	0.015	Frequently alternating cross-section
$n_3$	0.02	Minor obstruction (< 15% channel area)
$n_4$	0.03	Large amount of vegetation
$m$	1.0	Sinuosity = 1 (for BdV model)
$n$	0.087	Manning’s $n$ in this model

Table 2: Values used to calculate Manning’s  $n$  for a theoretical straight channel.  $D_{50}$  is median grain diameter.

<sup>225</sup> Manning’s  $n$  is often estimated as the sum of five components times a  
<sup>226</sup> sinuosity factor  $m$ ,

$$n = m(n_b + n_1 + n_2 + n_3 + n_4) \quad (9)$$

<sup>227</sup> where  $n_b$  is a base coefficient for a given boundary material, and  $m$  ranges  
<sup>228</sup> from 1 to 1.3 to account for the increased drag of meandering channels  
<sup>229</sup> (George and Schneider, 1989). Table 2 gives estimates for  $n_b$  and  $n_1$  through  
<sup>230</sup>  $n_4$  used in this study, which resulted in a characteristic value of  $n = 0.087$   
<sup>231</sup> for a straight channel (letting  $m = 1$ ). This value was assumed constant  
<sup>232</sup> throughout the study area.

<sup>233</sup> *3.5. Hydrological submodel*

<sup>234</sup> Given the monthly event discharge  $Q_m^*$  and channel friction, the hydro-  
<sup>235</sup> logical submodel models monthly flow depth and bulk velocity. Manning’s

equation for steady, uniform, open-channel flow was used to estimate monthly flow depth  $H_m$ . Manning's equation can be written in terms of discharge as

$$Q = \frac{1}{n} \frac{A_c^{5/3}}{P^{2/3}} S^{1/2} \quad (10)$$

where  $A_c$  is cross-sectional area ( $\text{m}^2$ ),  $P$  is wetted perimeter (m),  $S$  is longitudinal slope ( $\text{m/m}$ ), and  $n$  is Manning's roughness coefficient. For a rectangular channel cross-section, expanding the components for  $A_c$  and  $P$  yields

$$Q = \frac{1}{n} \frac{(BH_n)^{5/3}}{(B + 2H_n)^{2/3}} S^{1/2} \quad (11)$$

where  $H_n$  is the so-called normal depth, i.e., the depth that corresponds to a given discharge, roughness, width, and slope under the assumptions of steady uniform flow. Equation (11) can be solved for  $H_n$  using a variety of methods (Vatankhah, 2013). Here, Equation (11) was solved using Newton's method (Tiwari et al., 2012). For each month, bulk velocity was calculated as  $U = Q^*/(BH_n)$ .

### 3.6. Hydrodynamic model

The hydrodynamic submodel drives the streambank erosion model by providing the near-bank velocity excess  $\Delta U$  (Equation (1)). In the hydrodynamic model of Blanckaert and de Vriend (2010), the downstream velocity width-distribution, which leads to near-bank velocity perturbations, is parameterized by  $\alpha_s/R$ , where  $\alpha_s = -1$  corresponds to a potential vortex distribution and  $\alpha_s = 1$  to a forced vortex distribution. In straight reaches,  $\alpha_s$  is near zero and near-bank velocity is close to the average velocity (Blanckaert and de Vriend, 2003). The streamwise development of  $\alpha_s/R$  is represented by a relaxation equation. The relaxation equation has an adaptation length

largely controlled by  $C_f^{-1}H/R$ , and driving mechanisms representing transverse slope, curvature forcing, secondary flow, and velocity redistribution by the secondary flow (Blanckaert and de Vriend, 2010, equation 37). Near-bank depth excess  $\Delta h$  is induced by basal scour and is given by  $(HA)/R$ . The  $A/R$  term parameterizes transverse bed slope and is also represented by a relaxation equation with an adaptation length dependent on  $H$  and  $C_f$  (Blanckaert and de Vriend, 2010, equation 20). The scour factor  $A$  was here assumed to be 3, which represents a typical value for natural rivers (Ottevanger et al., 2012).

The near-bank values of  $\Delta U$  and  $\Delta h$  were obtained throughout each reach

$$\Delta U = U_s \frac{\alpha_s}{R} \frac{B}{2} \quad (12)$$

$$\Delta h = H \frac{A}{R} \frac{B}{2} \quad (13)$$

where  $U_s$  is the downstream bulk velocity and  $H$  is the cross-sectional average flow depth. Bank height was computed as  $H_b = H + \Delta h$ . Because the model of this paper does not make any assumptions about the accretion of the opposite bank,  $\Delta U$  is subsequently set to zero at locations where it is modeled to be negative.

The BdV model was run on a monthly timestep by varying the monthly event discharge and flow depth according to the procedure detailed above. Prior to the initial model simulation of each channel, bankfull discharge and flow depth conditions were simulated to set the initial bed geometry, and this geometry was held constant throughout subsequent monthly simulations. Source code for BdV was provided by Ottevanger et al. (2013) through the OpenEarth repository (<https://publicwiki.deltares.nl/display/>)

278 OET/OpenEarth).

279 *3.7. Soil erodibility data*

280 Soil erodibility was modeled using  $K_1$  (Equation (3)) and  $K_2$  (Equation (4)). Area- and depth-weighted average bulk density was obtained from the SSURGO dataset in the form of a 10 m raster (Wieczorek, M. E., USGS Data Series 866, [http://water.usgs.gov/GIS/metadata/usgswrd/XML/ds866\\_ssurgo\\_variables.xml](http://water.usgs.gov/GIS/metadata/usgswrd/XML/ds866_ssurgo_variables.xml)). Root density  $RD$  was modeled as a function of tree cover  $TC$  and bank height  $H_b$  (Equation (5)). Tree cover was obtained as a 30 m raster from the Global Land Cover Facility at the University of Maryland (Sexton et al., 2013). This dataset is based on Landsat observations, is free to the public, covers the entire globe, and is readily available online (<http://www.landcover.org/data/landsatTreecover/>). Three datasets are available based on observations from 2000, 2005, and 2010. Although erosion rates were measured during 2014–2016, the 2010 raster contains many small gaps associated with cloud cover. Therefore, the 2005 raster was used. This dataset seems to match the tree cover at all of the erosion sites used for calibration, at least qualitatively. One exception is Sconnier’s Mill Creek (sites SM01 and SM02), which has recently lost much of its tree cover in a limited area near the bank. Based on our field experience, an estimated value of 5% was assigned as input for this location. All other locations used values from the 2005 tree cover raster.

299 **4. GIS environment**

300 The raster data representing tree cover, bulk density, and monthly streamflow and the polylines representing channel geometry were managed in a ge-

Parameter		Data source	Reference	Processing
Monthly streamflow	$Q_m$	NLDAS-2 Noah	Xia et al. (2012)	Basin accumulate
Monthly storm freq.	$f_m$	PRISM	Rossi et al. (2016)	Wet days/total
Tree cover	$TC$	GLCF	Sexton et al. (2013)	—
Bulk density	$\rho_b$	SSURGO	USGS Data Series 866	Weighted avg.

SR: surface reflectance.

GLCF: Global Land Cover Facility, The University of Maryland ([www.landcover.org](http://www.landcover.org)).

SSURGO: Soil Survey Geographic Database (USDA).

PRISM: PRISM Climate Group, Oregon State University (<http://prism.oregonstate.edu>)

Table 3: Geospatial data sources and processing

302 geographic information system (GIS) using Matlab (Figure 5). The 30 m pixel  
 303 size of these raster data is relatively coarse compared to the studied channel  
 304 reaches. Errors can arise if the raster data are sampled at pixels represen-  
 305 tative of the opposite streambank or corresponding to the mid-channel open  
 306 water. Therefore, rasters were sampled at bank locations, rather than chan-  
 307 nel centerlines. Left- and right-bank locations were modeled as one channel  
 308 width from each centerline using the unit normal vectors  $n$  calculated during  
 309 PCS-interpolation of the channel centerline. To associate measured erosion  
 310 rates to a modeled bank location and channel centerline node, the GPS lo-  
 311 cations recorded in the field were matched with the nearest-neighbor bank  
 312 location (Figure 5).

313 Rasters were sampled at runtime by looping through the bank point lo-  
 314 cations and extracting (Matlab function *imread*) and interpolating the four  
 315 nearest pixels from the raster dataset. This approach has the advantage that  
 316 rasters of differing resolution and/or spatial references can be used without

317 the need to reproject the entire raster, provided that geotransforms exist  
 318 between the various spatial reference coordinates. This allows entire river  
 319 reaches to be modeled efficiently. Bilinear interpolation results in bank erodi-  
 320 bility estimates that vary smoothly throughout a meander bend, rather than  
 321 in sharp jumps characteristic of the raw raster pixels. Each bank location,  
 322 therefore, is assigned unique values of tree cover and bulk density as well as  
 323 a value of near-bank velocity excess and bank height from the hydrodynamic  
 324 model.

## 325 5. Results

326 The free parameters were estimated by nonlinear regression (Matlab func-  
 327 tion *fitnlm*). This function requires an explicit statement of the error model  
 328 structure (constant or proportional). For stochastic events such as stream-  
 329 bank erosion, variance is proportional to the maximum magnitude of indi-  
 330 vidual events (Pizzuto et al., 2010). Therefore, a proportional error model  
 331 was considered most appropriate, which is similar to the multiplicative error  
 332 model commonly used in modelling environmental processes (Xia et al., 2012;  
 333 ?).

334 Two separate models were run using the same input data: one with soil  
 335 erodibility as  $K_1$  and another with soil erodibility as  $K_2$ . Figure 6 plots  
 336 the results of statistical calibration of each model. For  $E = K_1$ , the fitted  
 337 equation,

$$\hat{\zeta}_1 = 0.0322 \exp [-1.030 \ln(TC) + 0.197H_b + 0.768BD^{2.5}] \overline{\Delta U} \quad (14)$$

338 explicitly states (between brackets) the exponential expression representing  
 339  $K_1$  (Wynn and Mostaghimi, 2006), with the first two terms parameterizing

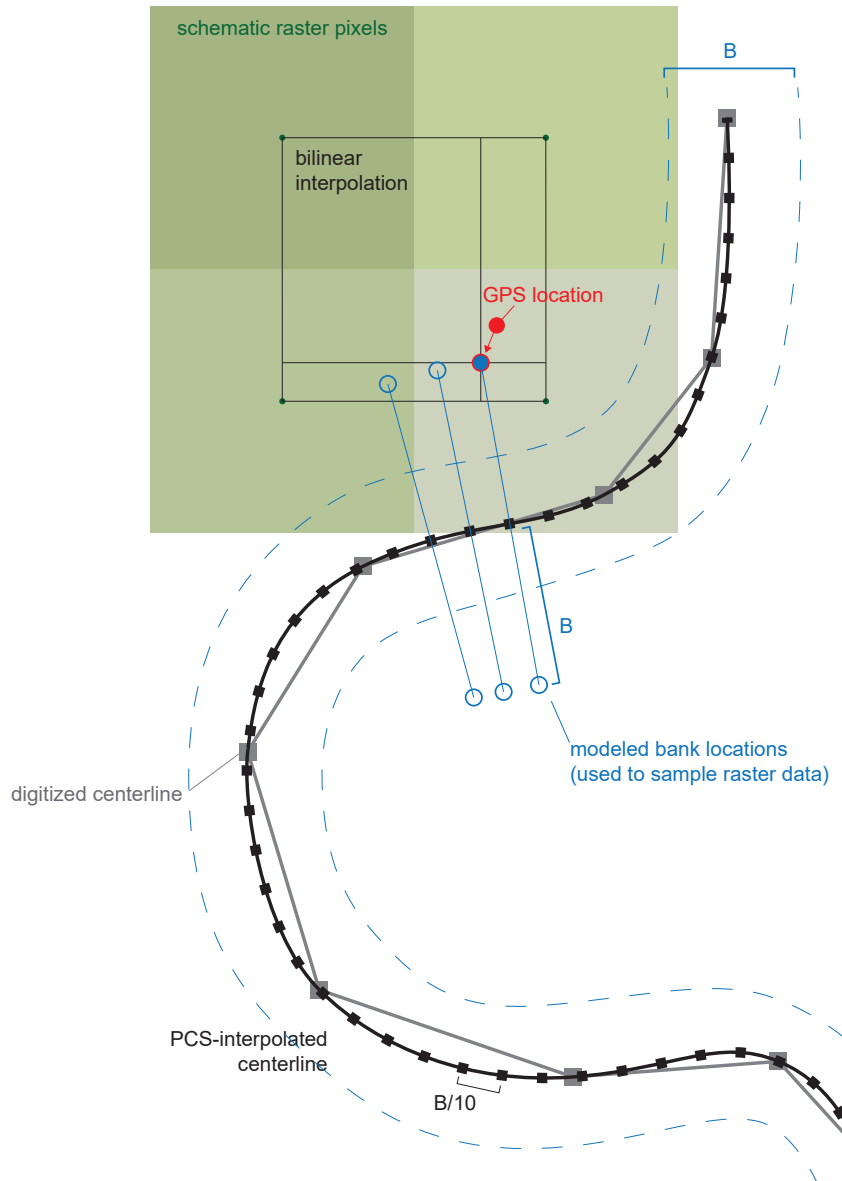


Figure 5: GIS environment. Centerlines digitized on a 3 m DEM (gray polyline) were PCS-interpolated (black). Banks locations (blue circles) were assumed  $B$  meters (channel width) from the centerline. The bank point nearest the cross-section as surveyed in the field (red circle) was selected. The 4 nearest raster pixels were interpolated (green squares).

340 coarse root density. Thus soil erodibility was predicted to be inversely re-  
341 lated to tree cover and directly related to bank height and bulk density. In  
342 contrast to this result, Wynn and Mostaghimi (2006) reported a strong in-  
343 verse relationship to bulk density. Possible reasons for this discrepancy are  
344 discussed below.

345 The simpler model incorporating  $E = K_2$ , in which soil erodibility is a  
346 function of bank height and tree cover only, is given by the fitted equation,

$$\hat{\zeta}_2 = 0.294 TC^{-1.05} \exp(0.157H_b)\overline{\Delta U} \quad (15)$$

347 which suggests that bank erosion rates are directly related to near-bank ve-  
348 locity excess and bank height and inversely related to tree cover. The coef-  
349 ficients and exponents are thus physically sound. Although the datapoints  
350 with measured streambank erosion rates equal to zero ( $n = 4$ ) are not shown  
351 on the log-log plots of Figure 6, they were also predicted by the models. Both  
352 models predicted erosion rates of zero for two of the four, i.e.,  $\overline{\Delta U} < 0$ . The  
353 model incorporating  $K_1$  predicted the other two to erode at 0.0079 m/yr and  
354 0.047 m/yr, a modest overestimate of  $\sim 1$  to 5 cm/yr. The model incorpo-  
355 rating  $K_2$  predicted negligible values of less than 0.001 m/yr for these two  
356 locations.

357 Figure 7 shows the results of applying the model with  $E = K_2$  to a  
358 medium-sized stream in a mixed pasture/forest landscape in Okaloosa County,  
359 FL. The simulation was run using the same input data used to train the  
360 model, including a monthly discharge time series of 24 months. A few bends  
361 are currently meandering out of the riparian buffer zone into pastured areas,  
362 where tree cover is very low. The tree cover dataset reproduced the transi-  
363 tion from forest on the eastern side of the image to pasture on the left side

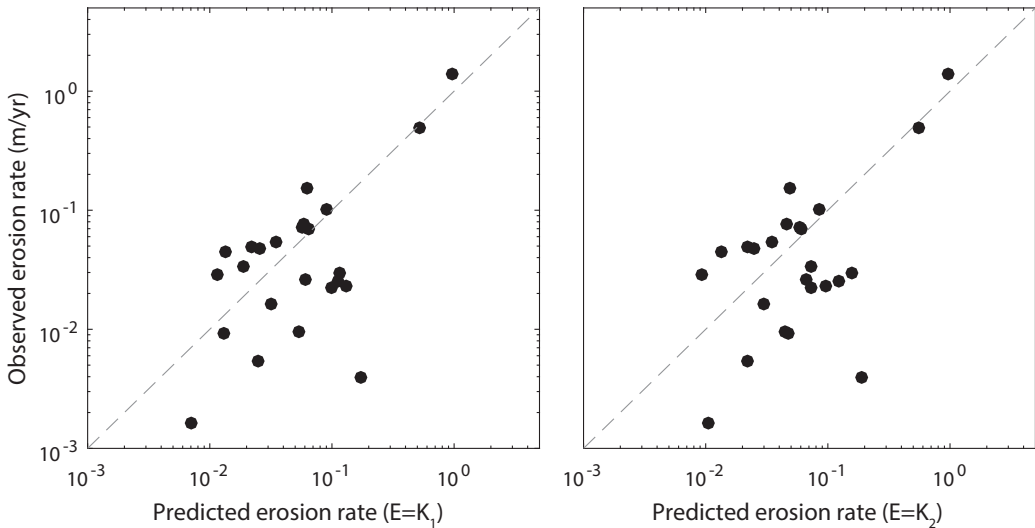


Figure 6: Results of model calibration using soil erodibility parameters  $K_1$  (Equation (3)) and  $K_2$  (Equation (4)). The model with  $K_1$  predicts streambank erosion rates with a significant correlation ( $R = 0.51, p = 0.008$ ). The model with  $K_2$  predicts streambank erosion rates slightly more accurately ( $R = 0.55, p = 0.005$ ) with fewer parameters. The dashed line is 1:1 correlation.

364 relatively accurately, though this is not quantified. Predicted streambank  
365 erosion rates throughout the reach are illustrated as thick colored lines. The  
366 original channel centerline, which was used in the model simulation, is shown  
367 as a thin line. The bank locations were shifted according to the predicted  
368 erosion rate to illustrate the amount of predicted bank retreat. Because the  
369 model only explicitly simulates bank retreat, not bank accretion, the shifted  
370 banks are shown only as a visualization of bank retreat, not as a quantitative  
371 prediction of channel migration.

372 Average streambank erosion rates are shown in colors ranging from black  
373 to yellow, corresponding to erosion rates up to 0.25 m/yr. Maximum erosion  
374 rates of >0.75 m/yr were predicted on the non-forested section of the large  
375 bend downstream (south) of the calibration locations (HH01 and HH02).  
376 This bend is also shown in Google Earth satellite imagery from March 2013.  
377 The satellite imagery allows qualitative comparisons to be made with the  
378 model simulation, but does not allow evaluation of the model's predictions,  
379 since the imagery is prior to the model simulation. The non-forested bends  
380 all host erosion rates of well over 0.25 m/yr. Reasonably high erosion rates  
381 were not only confined to non-forested bends, however; the downstream limb  
382 of a sharp bend near the bottom of the image was predicted to erode up to  
383 0.25 m/yr, which is comparable to the non-forested bend near HH01.

## 384 6. Discussion

385 We presented two models that predicted streambank erosion rates (Fig-  
386 ure 6). Using only three free parameters, the model with  $E = K_2$  is signifi-  
387 cantly correlated to observed erosion rates ( $R = 0.55, p < 0.001$ ) and slightly

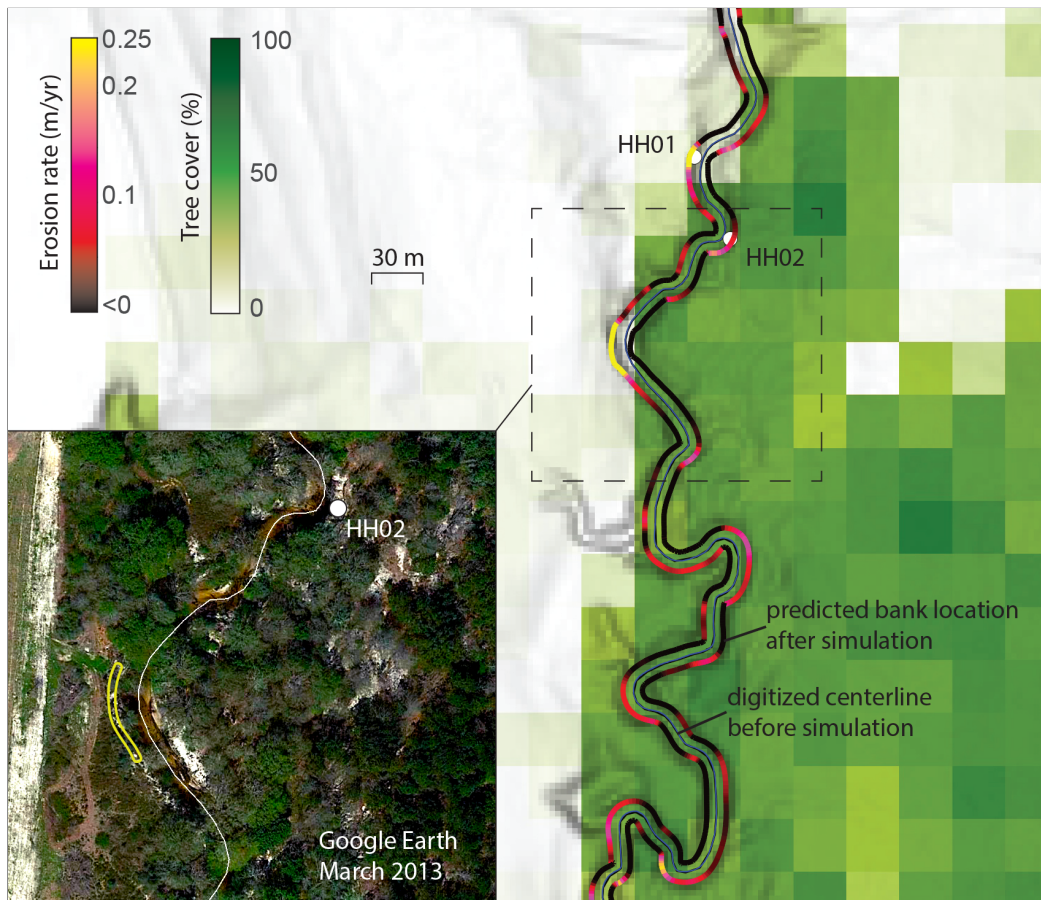


Figure 7: Predicted streambank erosion rates for Horsehead Creek. The predicted bank locations after erosion are colored by erosion rate (0–25 cm/yr). Light to dark shading is topographic slope from the 3 m DEM. HH01 and HH02: bank erosion monitoring/calibration locations. Inset: Google Earth image showing location of HH02 and a zone of predicted high erosion (75 cm/yr) on a downstream bend (yellow area).

more accurate than the model incorporating  $K_1$ , which adds a term representing soil bulk density. The negative relationship between bulk density and bank erosion reported by (Wynn and Mostaghimi, 2006) was not observed here. This could be due to many factors. Soils with high organic matter and root biomass content would express lower bulk densities despite being less erodible overall, and sandy soils commonly express higher bulk densities as well as higher erodibility. The large-scale SSURGO dataset may also be unable to resolve the spatial heterogeneity of bank materials, especially for many of the small channels used to calibrate the model. This result agrees with recent work by Daly et al. (2015), who found that watershed-scale relationships for bank erodibility based on soil properties showed no significant correlations to erodibility coefficient or critical shear stress. It is therefore not surprising that  $K_1$  did not improve the bank erodibility estimation across the many watersheds of our study.

The overall effectiveness of  $K_2$  agrees with the observations of Pizzuto (1984); Pizzuto and Meckelnburg (1989); Pizzuto et al. (2010), who found that forested streambank erodibility is largely controlled by tree density. Assuming representative values of tree cover of 5–10% for pastured/agricultural areas and 40–60% for forested areas, Equation (15) predicts that forested streambanks retreat 4 to 12 times slower than non-forested ones. This generally agrees with previous studies, which have reported two to five-fold differences in bank erodibility between forested and non-forested streambanks (Allmendinger et al., 2005; Micheli et al., 2004; Sass and Keane, 2012). The relatively large (up to 12-fold) difference implied here is probably due to the extremely low erosion rates of forested streambanks in these low-gradient

413 coastal plain streams, rather than especially high erosion rates of non-forested  
414 streambanks.

415 In both models, there appear to be two distinct groups of data points, one  
416 with largely positive residuals and another with negative residuals. Residuals  
417 were mapped and Moran's Index of  $I = -0.09$  was calculated in ArcMap,  
418 indicating that the residuals are not spatially autocorrelated and are not  
419 statistically different from random ( $p = 0.86$ ). Figure 8 maps the residuals  
420 over Noah-2.8 surface runoff and PRISM precipitation totals for September  
421 2015. Comparison to the PRISM data shows that some highly localized  
422 but intense storms were not represented well in the Noah-2.8 runoff sim-  
423 ulations, either as a result of the coarse resolution of the NLDAS-2 forc-  
424 ing data, or because of inaccuracies in the Noah-2.8 LSM. Extreme rain-  
425 fall totals and flash flooding were documented by weather stations in the  
426 area during this event (National Weather Service, North Central Gulf Coast  
427 Heavy Rain Event 27-29 September 2015, accessed 16 June 2016, [https://www.weather.gov/mob/heavyrain\\_sep2015](https://www.weather.gov/mob/heavyrain_sep2015)). It is likely that the Noah-2.8  
428 underestimated surface runoff during such small intense storms, which may  
429 have contributed to the negative residuals shown on the map (Figure 8).

431 It would be useful to compare the model of this paper to similar mod-  
432 els in the literature, but few if any comparable models exist. One spatially  
433 distributed model for total sediment yield from drainage basins, SedNet,  
434 quantifies streambank annual streambank erosion as a function of bankfull  
435 stream power, bank erodibility, and a daily streamflow factor (Wilkinson  
436 et al., 2014, 2009). The SedNet model requires a long-term dataset of daily  
437 streamflow observations as well as rasters representing vegetation cover and

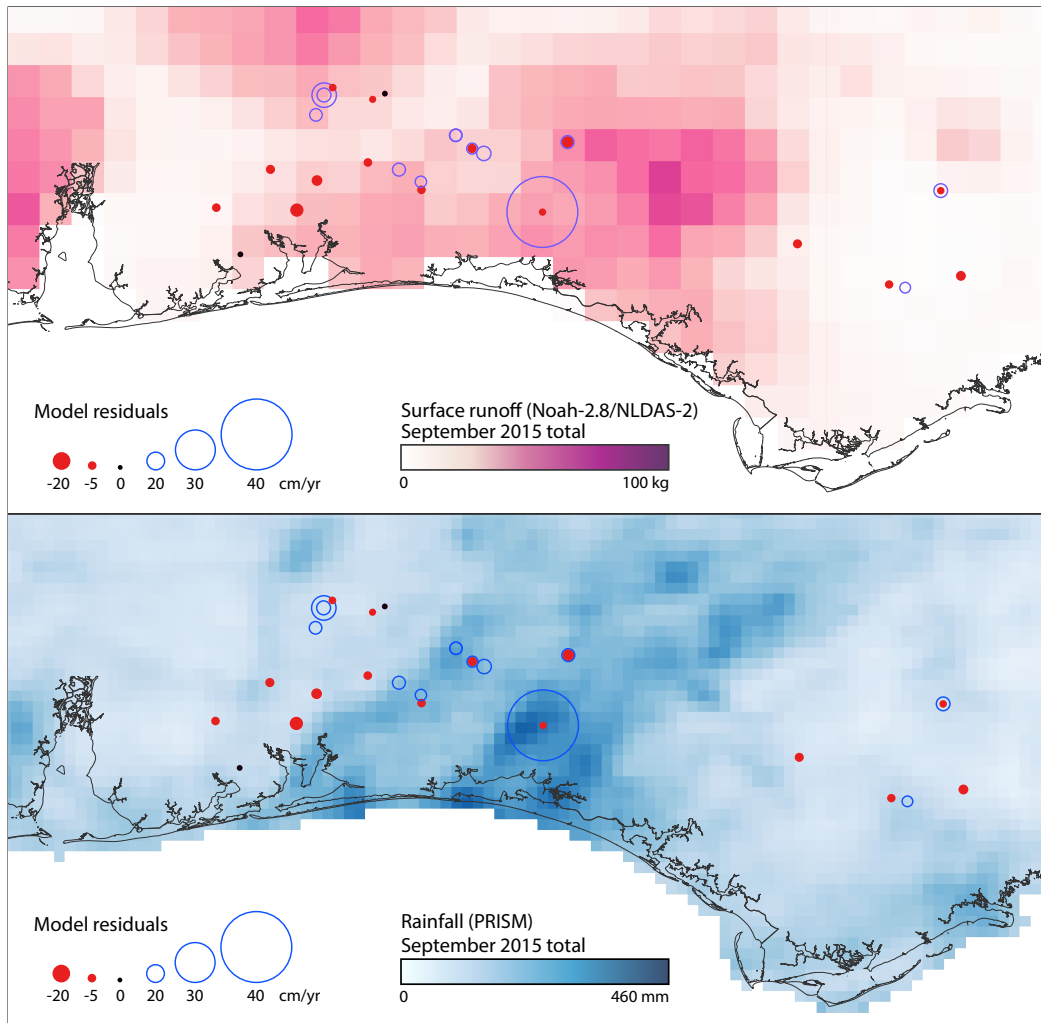


Figure 8: Map of residuals. Comparison of Noah-2.8 surface runoff (top) and PRISM precipitation (bottom) for September 2015 demonstrates discrepancies in the Noah model. A small but intense storm near the middle of the map is not represented in the surface runoff data.

438 soil vs. bedrock. Rather than modelling the spatial variability introduced  
439 by hydrodynamic processes, SedNet models the average bank erosion of en-  
440 tire stream links. SedNet was not designed to allow the prediction of local  
441 streambank erosion rates, or the identification of erosion hot-spots, but rather  
442 to simulate the large-scale processes exporting sediment from large drainage  
443 basins; streambank erosion is just one part of the model. Nevertheless, it is  
444 increasingly being used to estimate local streambank erosion rates because  
445 it is the only spatially distributed model that attempts to do so (Bartley  
446 et al., 2008). One recent evaluation of the accuracy of the streambank ero-  
447 sion rates predicted by SedNet showed that its original predictions differed  
448 from measured erosion rates (averaged over 10 locations) by a factor of 74,  
449 but this discrepancy was decreased to a factor of  $\sim 2$  with calibration to  
450 field-measured values of bed slope and bankfull discharge.

451 The main goal of this paper was to develop a spatially distributed model  
452 that incorporated widely available data and could be readily used in practical  
453 applications. This approach necessitated a few simplifications. Manning's  $n$   
454 for a straight channel was assumed to be constant throughout the study  
455 area and throughout a channel cross-section, and the hydrodynamic model  
456 calculated a friction factor for each channel based on this estimate and flow  
457 depth. Natural channels are sure to express more variability in roughness  
458 due to bedforms, large woody debris, vegetation density, and the overall  
459 shape of the channel cross-section. Nonetheless, the approach described here  
460 for estimating Manning's  $n$  resulted in realistic values of channel roughness  
461 and successful model simulations. Values of channel friction that are too  
462 large cause the hydrodynamic calculations to diverge, while values that are

463 too low lead to unrealistic simulations. The values resulting from letting  
464  $n = 0.087$  for a straight channel resulted in realistic flow patterns. The  
465 model's simulations should improve with reach-specific measurements of  $n$ ,  
466 but this remains to be tested.

467 Another limitation of the model is its reliance on an *ad hoc* method  
468 for determining the relevant monthly discharge, which was estimated as a  
469 function of average monthly discharge and storm frequency. The lack of  
470 streamgages in the basins being studied necessitated modelling of monthly  
471 streamflow. The average monthly streamflow estimates are from the Noah-2.8  
472 LSM, a large-scale land surface model designed to simulate processes acting  
473 at the global, continental, and large watershed scale. Such models have been  
474 shown to be relatively inaccurate at predicting streamflow in small basins,  
475 though they often express a higher skill in the southeastern U.S. than in other  
476 regions (Xia et al., 2012). Nevertheless, the Noah-2.8 output with NLDAS-2  
477 forcings has global coverage and is provided in near real-time at the Land  
478 Data Assimilation Systems of NASA's Goddard Space Flight Center (<http://ldas.gsfc.nasa.gov/nldas/>). The spatial resolution of NLDAS-2 output is  
479 currently  $1/8^\circ$  but may improve with the release of NLDAS-3, which may  
480 allow flow routing in many small to medium size basins. The model of this  
481 paper can only improve as the community improves the accuracy and spatial  
482 resolution of global LSMs. Future work could integrate the hydrodynamic  
483 model with the hourly output from LSMs, or with discharge measurements  
484 from gaged watersheds.  
485

486 **7. Conclusions**

487 Bartley et al. (2008) remarked that “it will be difficult for catchment scale  
488 sediment budget models to ever accurately predict the location and rate of  
489 bank erosion due to the variation in bank erosion rates in both space and  
490 time.” de Vente et al. (2013) cited the lack of a bank erosion component as  
491 a major limitation of current sediment detachment models. We presented  
492 a spatially distributed model for streambank erosion incorporating a sim-  
493 ple soil erodibility parameter ( $K_2$ ), a nonlinear hydrodynamic model, and  
494 monthly discharge forcings. An application of the model to a medium-sized  
495 stream in the Gulf Coastal plain (Figure 7) demonstrated its potential for  
496 quantifying annual streambank erosion throughout a mixed forest/pasture  
497 reach. Although future work should focus on improving the model’s parame-  
498 terization of roughness and streamflow, the current model shows a significant  
499 ( $p = 0.002$ ) correlation to observed erosion rates ( $R = 0.55$ ). The model thus  
500 represents a first step in filling the long-standing gap emphasized by Bartley  
501 et al. (2008) and de Vente et al. (2013). The calibrated model can be used to  
502 predict erosion rates throughout the northern Gulf of Mexico coastal plain,  
503 or the model can be calibrated for use in other regions.

504 **8. Acknowledgments**

505 We thank David Cambron and Michele Goodfellow for their help in col-  
506 lecting data for this study. This study was based on work supported by a  
507 grant from the Florida Fish and Wildlife Conservation Commission and the  
508 U.S. Fish and Wildlife Service (State Wildlife Grant 13058). The Geological  
509 Society of America, the Gulf Coast Association of Geological Societies, and

510 the University of West Florida Scholarly and Creative Activities Committee  
511 provided additional funding.

512 **References**

- 513 Allmendinger, N. E., Pizzuto, J. E., Potter, N., Johnson, T. E., Hession,  
514 W. C., 2005. The influence of riparian vegetation on stream width, eastern  
515 Pennsylvania, USA. Geological Society of America Bulletin 117 (1), 229.  
516 URL <http://gsabulletin.gsapubs.org/cgi/doi/10.1130/B25447.1>
- 517 Bandyopadhyay, S., Ghosh, K., De, S. K., 2014. A proposed method of  
518 bank erosion vulnerability zonation and its application on the River Haora,  
519 Tripura, India. Geomorphology 224, 111–121.  
520 URL <http://linkinghub.elsevier.com/retrieve/pii/S0169555X14003821>
- 521 Bartley, R., Keen, R. J., Hawdon, A. A., Hairsine, P. B., Disher, M. G.,  
522 Kinsey-Henderson, A. E., 2008. Bank erosion and channel width change  
523 in a tropical catchment. Earth Surface Processes and Landforms 33 (14),  
524 2174–2200.  
525 URL <http://www3.interscience.wiley.com/journal/121517813/abstract>
- 526 Bieger, K., Rathjens, H., Allen, P. M., Arnold, J. G., 2015. Development  
527 and evaluation of bankfull hydraulic geometry relationships for the phys-  
528 iographic regions of the United States. Journal of the American Water  
529 Resources Association 51 (3), 842–858.
- 530 Blanckaert, K., de Vriend, H. J., 2003. Nonlinear modeling of mean flow  
531 redistribution in curved open channels. Water Resources Research 39 (12),  
532 1375.

- 533 Blanckaert, K., de Vriend, H. J., 2010. Meander dynamics: A nonlinear model  
534 without curvature restrictions for flow in open-channel bends. *Journal of*  
535 *Geophysical Research: Earth Surface* 115, F04011.
- 536 Bull, L. J., 1997. Magnitude and variation in the contribution of bank erosion  
537 to the suspended sediment load of the River Severn, UK. *Earth Surface*  
538 *Processes and Landforms* 22 (12), 1109–1123.
- 539 Camporeale, C., Perona, P., Porporato, A., Ridolfi, L., 2007. Hierarchy of  
540 models for meandering rivers and related morphodynamic processes. *Re-*  
541 *views of Geophysics* 45 (1), 5–28.  
542 URL <http://doi.wiley.com/10.1029/2005RG000185>
- 543 Couper, P. R., 2003. Effects of siltclay content on the susceptibility of river  
544 banks to subaerial erosion. *Geomorphology* 56 (1-2), 95–108.  
545 URL <http://linkinghub.elsevier.com/retrieve/pii/S0169555X03000485>
- 546 Crosato, A., 2009. Physical explanations of variations in river meander migra-  
547 tion rates from model comparison. *Earth Surface Processes and Landforms*  
548 34 (15), 2078–2086.  
549 URL <http://www3.interscience.wiley.com/journal/121517813/abstract>
- 550 Daly, E. R., Miller, R. B., Fox, G. A., 2015. Modeling streambank erosion and  
551 failure along protected and unprotected composite streambanks. *Advances*  
552 *in Water Resources* 81, 114–127.  
553 URL <http://linkinghub.elsevier.com/retrieve/pii/S0309170815000068>
- 554 de Vente, J., Poesen, J., Verstraeten, G., Govers, G., Vanmaercke, M., Van  
555 Rompaey, A., Arabkhedri, M., Boix-Fayos, C., 2013. Predicting soil erosion

- 556 and sediment yield at regional scales: Where do we stand? Earth-Science  
557 Reviews 127, 16–29.
- 558 URL <http://linkinghub.elsevier.com/retrieve/pii/S0012825213001475>
- 559 Dietrich, W., Bellugi, D., Sklar, L., Stock, J., Heimsath, A., Roering, J.,  
560 2003. Geomorphic transport laws for predicting landscape form and dy-  
561 namics. In: Wilcock, P., Iverson, R. (Eds.), Prediction in Geomorphology.  
562 Vol. 135 of Geophysical Monograph Series. American Geophysical Union,  
563 Washington, DC, pp. 103–132.
- 564 URL <http://onlinelibrary.wiley.com/doi/10.1029/135GM09/summary>
- 565 Dietrich, W., Smith, J., Dunne, T., 1979. Flow and sediment transport in a  
566 sand bedded meander. The Journal of Geology 87 (3), 305–315.
- 567 URL <http://www.jstor.org/stable/30060821>
- 568 Dietrich, W. E., Smith, J. D., 1983. Influence of the point bar on flow through  
569 curved channels. Water Resources Research 19 (5), 1173–1192.
- 570 URL <http://doi.wiley.com/10.1029/WR019i005p01173>
- 571 Eke, E., Parker, G., Shimizu, Y., 2014. Numerical modeling of erosional  
572 and depositional bank processes in migrating river bends with self-formed  
573 width: Morphodynamics of bar push and bank pull. Journal of Geophysical  
574 Research: Earth Surface 119, 1455–1483.
- 575 URL <http://onlinelibrary.wiley.com/doi/10.1002/2013JF003020/abstract>
- 576 Faustini, J. M., Kaufmann, P. R., Herlihy, A. T., 2009. Downstream variation  
577 in bankfull width of wadeable streams across the conterminous United

- 578 States. Geomorphology 108 (3-4), 292–311.
- 579 URL <http://linkinghub.elsevier.com/retrieve/pii/S0169555X09000762>
- 580 Florsheim, J. L., Mount, J. F., Chin, A., 2008. Bank erosion as a desirable  
581 attribute of rivers. BioScience 58 (6), 519–528.
- 582 George, A. J. J., Schneider, V. R., 1989. Guide for selecting Manning's rough-  
583 ness coefficients for natural channels and flood plains. U.S. Geological Sur-  
584vey Water-Supply Paper 2339.
- 585 Gregory, K., 2006. The human role in changing river channels. Geomorphol-  
586 ogy 79 (3-4), 172–191.
- 587 URL <http://linkinghub.elsevier.com/retrieve/pii/S0169555X06002509>
- 588 Güneralp, I., Filippi, A., Hales, B., 2013. River-flow boundary delineation  
589 from digital aerial photography and ancillary images using Support Vector  
590 Machines. GIScience & Remote Sensing 50 (1), 1–25.
- 591 URL <http://www.tandfonline.com/doi/abs/10.1080/15481603.2013.778560>
- 593 Güneralp, I., Filippi, A. M., Randall, J., 2014. Estimation of floodplain  
594 aboveground biomass using multispectral remote sensing and nonpara-  
595 metric modeling. International Journal of Applied Earth Observation and  
596 Geoinformation 33, 119–126.
- 597 URL <http://linkinghub.elsevier.com/retrieve/pii/S0303243414001160>
- 598 Güneralp, I., Rhoads, B. L., 2007. Continuous characterization of the plan-  
599 form geometry and curvature of meandering rivers. Geographical Analysis

- 600 40 (1), 1–25.
- 601 URL <http://doi.wiley.com/10.1111/j.0016-7363.2007.00711.x>
- 602 Harmel, R., Haan, C., Dutnall, R., 1999. Evaluation of Rosgen's stream-  
603 bank erosion potential assessment in Northeast Oklahoma. *Journal of the  
604 American Water Resources Association* 35 (1), 113–121.
- 605 Hooke, J. M., 1980. Magnitude and distribution of rates of river bank erosion.  
606 *Earth Surface Processes and Landforms* 5, 143–157.
- 607 Hooke, R., 1975. Distribution of sediment transport and shear stress in a  
608 meander bend. *The Journal of Geology* 83 (5), 543–565.  
609 URL <http://www.jstor.org/stable/30061053>
- 610 Hubble, T. C. T., Docker, B. B., Rutherford, I. D., 2010. The role of riparian  
611 trees in maintaining riverbank stability: A review of Australian experience  
612 and practice. *Ecological Engineering* 36 (3), 292–304.
- 613 Hupp, C. R., Simon, A., 1991. Bank accretion and the development of vege-  
614 tated depositional surfaces along modified alluvial channels. *Geomorphol-  
615 ogy* 4 (2), 111–124.
- 616 Ikeda, S., Parker, G., Sawai, K., 1981. Bend theory of river meanders. Part  
617 1. Linear development. *Journal of Fluid Mechanics* 112, 363–377.  
618 URL [http://www.journals.cambridge.org/abstract\\_S0022112081000451](http://www.journals.cambridge.org/abstract_S0022112081000451)
- 619 Julian, J. P., Torres, R., 2006. Hydraulic erosion of cohesive riverbanks.  
620 *Geomorphology* 76 (1-2), 193–206.  
621 URL <http://linkinghub.elsevier.com/retrieve/pii/S0169555X0500365X>

- 622 Kemp, J., Olley, J., Ellison, T., McMahon, J., 2016. River response to Eu-  
623 ropean settlement in the subtropical Brisbane River, Australia. Anthro-  
624 pocene.
- 625 Knox, J. C., 2006. Floodplain sedimentation in the Upper Mississippi Valley:  
626 Natural versus human accelerated. *Geomorphology* 79 (3-4), 286–310.
- 627 Konsoer, K. M., Rhoads, B. L., Langendoen, E. J., Best, J. L., Ursic, M. E.,  
628 Abad, J. D., Garcia, M. H., 2016. Spatial variability in bank resistance to  
629 erosion on a large meandering, mixed bedrock-alluvial river. *Geomorphol-*  
630 *ogy* 252, 80–97.  
631 URL <http://dx.doi.org/10.1016/j.geomorph.2015.08.002>
- 632 Kronvang, B., Andersen, H. E., Larsen, S. E., Audet, J., 2013. Importance  
633 of bank erosion for sediment input, storage and export at the catchment  
634 scale. *Journal of Soils and Sediments* 13 (1), 230–241.
- 635 Kwan, H., Swanson, S., 2014. Prediction of Annual Streambank Erosion  
636 for Sequoia National Forest, California. *Journal of the American Water  
637 Resources Association* 50 (6), 1439–1447.  
638 URL <http://doi.wiley.com/10.1111/jawr.12200>
- 639 Lawler, D. M., 1993. The measurement of river bank erosion and lateral  
640 channel change: A review. *Earth Surface Processes and Landforms* 18 (9),  
641 777–821.  
642 URL <http://doi.wiley.com/10.1002/esp.3290180905>
- 643 Lawler, D. M., Grove, J. R., Couperthwaite, J. S., Leeks, G. J. L., 1999.

- 644 Downstream change in river bank erosion rates in the Swale-Ouse system,  
645 northern England. *Hydrological Processes* 13 (7), 977–992.
- 646 Lawler, D. M., Thorne, C. R., Hooke, J. M., 1997. Bank erosion and instabil-  
647 ity. In: Thorne, C. R., Hey, R. D., Newson, M. D. (Eds.), *Applied Fluvial*  
648 *Geomorphology for River Engineering and Management*. John Wiley &  
649 Sons Ltd., Chichester, pp. 137–172.
- 650 Leopold, L. B., Wolman, M. G., 1960. River meanders. *Geological Society*  
651 *of America Bulletin* 71 (6), 769–793.  
652 URL <http://gsabulletin.gsapubs.org/content/71/6/769>.shorthtpp:  
653 [/gsabulletin.gsapubs.org/cgi/doi/10.1130/0016-7606\(1960\)71\[769:RM\]2.0.CO;2](http://gsabulletin.gsapubs.org/cgi/doi/10.1130/0016-7606(1960)71[769:RM]2.0.CO;2)
- 655 Lyons, N. J., Starek, M. J., Wegmann, K. W., Mitasova, H., 2015. Bank  
656 erosion of legacy sediment at the transition from vertical to lateral stream  
657 incision. *Earth Surface Processes and Landforms* 40 (13), 1764–1778.
- 658 Matsubara, Y., Howard, A. D., 2014. Modeling planform evolution of a mud-  
659 dominated meandering river: Quinn River, Nevada, USA. *Earth Surface*  
660 *Processes and Landforms* 39 (10), 1365–1377.  
661 URL <http://doi.wiley.com/10.1002/esp.3588>
- 662 McMillan, M., 2016. Evaluating and developing streambank erosion models  
663 in the Gulf of Mexico Coastal Plain. Ph.D. thesis, The University of West  
664 Florida.
- 665 Merritts, D. J., Walter, R. C., Rahnis, M., Hartranft, J., Cox, S., Gellis,  
666 A., Potter, N., Hilgartner, W., Langland, M., Manion, L., Lippincott, C.,

- 667 Siddiqui, S., Rehman, Z., Scheid, C., Kratz, L., Shilling, A., Jenschke,  
668 M., Datin, K., Cranmer, E., Reed, A., Matuszewski, D., Voli, M., Ohlson,  
669 E., Neugebauer, A., Ahamed, A., Neal, C., Winter, A., Becker, S., 2011.  
670 Anthropocene streams and base-level controls from historic dams in the  
671 unglaciated mid-Atlantic region, USA. Philosophical Transactions of the  
672 Royal Society A: Mathematical, Physical, and Engineering Sciences 369,  
673 976–1009.
- 674 URL <http://www.ncbi.nlm.nih.gov/pubmed/21282157>
- 675 Metcalf, C. K., Wilkerson, S. D., Harman, W. A., 2009. Bankfull regional  
676 curves for North and Northwest Florida streams. Journal of the American  
677 Water Resources Association 45 (5), 1260–1272.
- 678 URL <http://doi.wiley.com/10.1111/j.1752-1688.2009.00364.x>
- 679 Micheli, E. R., Kirchner, J. W., 2002. Effects of wet meadow riparian vegeta-  
680 tion on streambank erosion. 2. Measurements of vegetated bank strength  
681 and consequences for failure mechanics. Earth Surface Processes and Land-  
682 forms 27 (7), 687–697.
- 683 URL <http://doi.wiley.com/10.1002/esp.340>
- 684 Micheli, E. R., Kirchner, J. W., Larsen, E. W., 2004. Quantifying the effect  
685 of riparian forest versus agricultural vegetation on river meander migra-  
686 tion rates, central Sacramento River, California, USA. River Research and  
687 Applications 20 (5), 537–548.
- 688 URL <http://doi.wiley.com/10.1002/rra.756>
- 689 Mitchell, K. E., Lohmann, D., Houser, P. R., Wood, E. F., Schaake, J. C.,  
690 Robock, A., Cosgrove, B. A., Sheffield, J., Duan, Q., Luo, L., Higgins,

- 691 R. W., Pinker, R. T., Tarpley, J. D., Lettenmaier, D. P., Marshall, C. H.,  
692 Entin, J. K., Pan, M., Shi, W., Koren, V., Meng, J., Ramsay, B. H., Bailey,  
693 A. A., 2004. The multi-institution North American Land Data Assimila-  
694 tion System (NLDAS): Utilizing multiple GCIP products and partners in  
695 a continental distributed hydrological modeling system. *Journal of Geo-  
696 physical Research* 109, D07S90.
- 697 URL <http://dx.doi.org/10.1029/2003JD003823>
- 698 Mosselman, E., 2014. Five common mistakes in fluvial morphodynamic mod-  
699 elling. *Advances in Water Resources* 16, 6329.  
700 URL <http://dx.doi.org/10.1016/j.advwatres.2015.07.025>
- 701 Odgaard, A. J., 1987. Streambank erosion along two rivers in Iowa. *Water  
702 Resources Research* 23 (7), 1125–1236.
- 703 Odgaard, A. J., 1989. River-meander model. II: Applications. *Journal of  
704 Hydraulic Engineering* 115 (11), 1451–1464.  
705 URL [http://ascelibrary.org/doi/10.1061/\(ASCE\)0733-9429\(1989\)115:11\(1451\)](http://ascelibrary.org/doi/10.1061/(ASCE)0733-9429(1989)115:11(1451))
- 707 Osman, A. M., Thorne, C. R., 1988. Riverbank Stability Analysis. I: Theory.  
708 *Journal of Hydraulic Engineering* 114 (2), 134–150.  
709 URL [http://ascelibrary.org/doi/abs/10.1061/\(ASCE\)0733-9429\(1988\)114:2\(134\)](http://ascelibrary.org/doi/abs/10.1061/(ASCE)0733-9429(1988)114:2(134))
- 711 Ottevanger, W., Blanckaert, K., Uijttewaal, W. S. J., 2012. Processes govern-  
712 ing the flow redistribution in sharp river bends. *Geomorphology* 163–164,

- 713 45–55.
- 714 URL <http://dx.doi.org/10.1016/j.geomorph.2011.04.049>
- 715 Ottevanger, W., Blanckaert, K., Uijttewaal, W. S. J., de Vriend, H. J., 2013.
- 716 Meander dynamics: A reduced-order nonlinear model without curvature
- 717 restrictions for flow and bed morphology. *Journal of Geophysical Research:*
- 718 *Earth Surface* 118, 1118–1131.
- 719 Parker, G., Shimizu, Y., Wilkerson, G. V., Eke, E. C., Abad, J. D., Lauer,
- 720 J. W., Paola, C., Dietrich, W. E., Voller, V. R., 2011. A new framework
- 721 for modeling the migration of meandering rivers. *Earth Surface Processes*
- 722 and Landforms 36 (1), 70–86.
- 723 URL <http://doi.wiley.com/10.1002/esp.2113>
- 724 Partheniades, E., 1965. Erosion and deposition of cohesive soils. *Journal of*
- 725 *the Hydraulics Division of the American Society of Civil Engineers* 91 (1),
- 726 105–139.
- 727 Pelletier, J. D., 2012. A spatially distributed model for the long-term sus-
- 728 pended sediment discharge and delivery ratio of drainage basins. *Journal*
- 729 *of Geophysical Research* 117, F02028.
- 730 URL <http://doi.wiley.com/10.1029/2011JF002129>
- 731 Pelletier, J. D., Brad Murray, A., Pierce, J. L., Bierman, P. R., Breshears,
- 732 D. D., Crosby, B. T., Ellis, M., Foufoula-Georgiou, E., Heimsath, A. M.,
- 733 Houser, C., Lancaster, N., Marani, M., Merritts, D. J., Moore, L. J., Ped-
- 734 erson, J. L., Poulos, M. J., Rittenour, T. M., Rowland, J. C., Ruggiero, P.,
- 735 Ward, D. J., Wickert, A. D., Yager, E. M., 2015. Forecasting the response

- 736 of Earth's surface to future climatic and land use changes: A review of  
737 methods and research needs. *Earth's Future* 3 (7), 220–251.
- 738 URL <http://doi.wiley.com/10.1002/2014EF000290>
- 739 Perucca, E., Camporeale, C., Ridolfi, L., 2007. Significance of the ripar-  
740 ian vegetation dynamics on meandering river morphodynamics. *Water Re-  
741 sources Research* 43, W03430.
- 742 URL <http://doi.wiley.com/10.1029/2006WR005234>
- 743 Pizzuto, J. E., 1984. Bank erodibility of shallow sandbed streams. *Earth  
744 Surface Processes and Landforms* 9 (2), 113–124.
- 745 URL <http://dx.doi.org/10.1002/esp.3290090203>
- 746 Pizzuto, J. E., 2009. An empirical model of event scale cohesive bank profile  
747 evolution. *Earth Surface Processes and Landforms* 34 (9), 1234–1244.
- 748 URL <http://doi.wiley.com/10.1002/esp.1808>
- 749 Pizzuto, J. E., Meckelnburg, T. S., 1989. Evaluation of a linear bank erosion  
750 equation. *Water Resources Research* 25 (5), 1005–1013.
- 751 URL <http://doi.wiley.com/10.1029/WR025i005p01005>
- 752 Pizzuto, J. E., O'Neal, M., Stotts, S., 2010. On the retreat of forested, cohe-  
753 sive riverbanks. *Geomorphology* 116 (3-4), 341–352.
- 754 URL <http://linkinghub.elsevier.com/retrieve/pii/S0169555X09004735>
- 755 Pollen, N., 2007. Temporal and spatial variability in root reinforcement of  
756 streambanks: Accounting for soil shear strength and moisture. *Catena* 69,  
757 197–205.

- 758 Pollen, N., Simon, A., 2005. Estimating the mechanical effects of riparian  
759 vegetation on stream bank stability using a fiber bundle model. Water  
760 Resources Research 41, W07025.  
761 URL <http://doi.wiley.com/10.1029/2004WR003801>
- 762 Rosgen, D. L., 2001. A practical method of computing streambank erosion  
763 rate. In: Proceedings of the Seventh Federal Interagency Sedimentation  
764 Conference. Vol. 1. US Inter-agency Committee on Water Resources,  
765 Subcommittee on Sedimentation, Reno, Nevada, pp. 9–18.  
766 URL [http://www.wildlandhydrology.com/assets/Streambank\\_erosion\\_paper.pdf](http://www.wildlandhydrology.com/assets/Streambank_erosion_paper.pdf)
- 768 Rosgen, D. L., 2009. Watershed Assessment of River Stability and Sediment  
769 Supply, 2nd Edition. Wildland Hydrology, Fort Collins, Colorado.
- 770 Rossi, M. W., Whipple, K. X., Vivoni, E. R., 2016. Precipitation and evapo-  
771 transpiration controls on daily runoff variability in the contiguous United  
772 States and Puerto Rico. Journal of Geophysical Research: Earth Surface  
773 121, 128–145.  
774 URL <http://doi.wiley.com/10.1002/2015JF003446>
- 775 Sass, C. K., Keane, T. D., 2012. Application of Rosgen's BANCS model for  
776 NE Kansas and the development of predictive streambank erosion curves.  
777 Journal of the American Water Resources Association 48 (4), 774–787.  
778 URL <http://doi.wiley.com/10.1111/j.1752-1688.2012.00644.x>
- 779 Sekely, A., Mulla, D., Bauer, D., 2002. Streambank slumping and its contri-  
780 bution to the phosphorus and suspended sediment loads of the Blue Earth

- 781 River, Minnesota. Journal of Soil and Water Conservation 57 (5), 243–250.
- 782 URL <http://www.jswconline.org/content/57/5/243.short>
- 783 Sexton, J. O., Song, X.-P., Feng, M., Noojipady, P., Anand, A., Huang, C.,  
784 Kim, D.-H., Collins, K. M., Channan, S., Dimiceli, C., Townshend, J. R.,  
785 2013. Global, 30-m resolution continuous fields of tree cover: Landsat-  
786 based rescaling of MODIS Vegetation Continuous Fields with lidar-based  
787 estimates of error. International Journal of Digital Earth 6 (5), 427–448.  
788 URL <http://dx.doi.org/10.1080/17538947.2013.786146>
- 789 Simon, A., Curini, A., Darby, S., Langendoen, E., 2000. Bank and near-bank  
790 processes in an incised channel. Geomorphology 35 (3-4), 193–217.  
791 URL <http://linkinghub.elsevier.com/retrieve/pii/S0169555X00000362>
- 792 Simon, A., Doyle, M., 2007. Critical evaluation of how the Rosgen classifi-  
793 cation and associated “Natural Channel Design” methods fail to integrate  
794 and quantify fluvial processes and channel response. Journal of the Amer-  
795 ican Water Resources Association 43 (5), 1117–1131.  
796 URL <http://onlinelibrary.wiley.com/doi/10.1111/j.1752-1688.2007.00091.x/full>
- 797 Stott, T., 1997. A comparison of stream bank erosion processes on forested  
798 and moorland streams in the Balquhidder Catchments, central Scotland.  
799 Earth Surface Processes and Landforms 22 (4), 383–399.  
800 URL [http://doi.wiley.com/10.1002/\(SICI\)1096-9837\(199704\)22:4<383::AID-ESP695>3.0.CO;2-4](http://doi.wiley.com/10.1002/(SICI)1096-9837(199704)22:4<383::AID-ESP695>3.0.CO;2-4)
- 801 Thomas, R. E., Pollen-Bankhead, N., 2010. Modeling root-reinforcement

- 804 with a fiber-bundle model and Monte Carlo simulation. Ecological En-  
805 gineering 36 (1), 47–61.
- 806 URL <http://linkinghub.elsevier.com/retrieve/pii/S092585740900250X>
- 807 Thorne, C., 1982. Processes and mechanisms of river bank erosion. In: Hey,  
808 Bathurst, J., Thorne, C. (Eds.), Gravel-Bed Rivers: Processes, Tools,  
809 Environments. Wiley, Chichester, England, pp. 227–271.
- 810 Thorne, S. D., Furbish, D. J., 1995. Influences of coarse bank roughness on  
811 flow within a sharply curved river bend. Geomorphology 12 (3), 241–257.
- 812 Tiwari, H., Das, P., Bharti, A. K., 2012. MATLAB programming solution for  
813 critical and normal depth in trapezoidal channels. International Journal of  
814 Engineering Research and Technology 1 (8), 1–3.
- 815 U.S. Environmental Protection Agency, 2000. National Water Quality Inven-  
816 tory.
- 817 Van Eps, M. A., Formica, S. J., Morris, T. L., Beck, J. M., Cotter, A. S., 2004.  
818 Using a bank erosion hazard index (BEHI) to estimate annual sediment  
819 loads from streambank erosion in the West Fork White River watershed.  
820 In: Self-Sustaining Solutions for Streams, Wetlands, and Watersheds, 12–  
821 15, September 2004. American Society of Agricultural and Biological En-  
822 gineers, American Society of Agricultural and Biological Engineers, St.  
823 Joseph, MI.
- 824 URL <http://elibrary.asabe.org/abstract.asp?JID=1&AID=17386&CID=sww2004&T=1>

- 826 Vatankhah, A. R., 2013. Explicit solutions for critical and normal depths in  
827 trapezoidal and parabolic open channels. Ain Shams Engineering Journal  
828 4 (1), 17–23.
- 829 Walter, R. C., Merritts, D. J., 2008. Natural streams and the legacy of water-  
830 powered mills. Science 319, 299–304.  
831 URL <http://www.sciencemag.org/cgi/doi/10.1126/science.1151716>
- 832 Wilkinson, S. N., Dougall, C., Kinsey-Henderson, A. E., Searle, R. D., Ellis,  
833 R. J., Bartley, R., 2014. Development of a time-stepping sediment budget  
834 model for assessing land use impacts in large river basins. Science of the  
835 Total Environment 468-469, 1210–1224.  
836 URL <http://dx.doi.org/10.1016/j.scitotenv.2013.07.049>
- 837 Wilkinson, S. N., Prosser, I. P., Rustomji, P., Read, A. M., 2009. Modelling  
838 and testing spatially distributed sediment budgets to relate erosion pro-  
839 cesses to sediment yields. Environmental Modelling and Software 24 (4),  
840 489–501.  
841 URL <http://dx.doi.org/10.1016/j.envsoft.2008.09.006>
- 842 Wynn, T. M., Mostaghimi, S., 2006. The effects of vegetation and soil  
843 type on streambank erosion, southwestern Virginia, USA. Journal of the  
844 American Water Resources Association 42 (1), 69–82.  
845 URL <http://onlinelibrary.wiley.com/doi/10.1111/j.1752-1688.2006.tb03824.x/abstract>  
846
- 847 Xia, Y., Mitchell, K., Ek, M., Cosgrove, B., Sheffield, J., Luo, L., Alonge, C.,  
848 Wei, H., Meng, J., Livneh, B., Duan, Q., Lohmann, D., 2012. Continental-

849 scale water and energy flux analysis and validation for North American  
850 Land Data Assimilation System project phase 2 (NLDAS-2): 2. Validation  
851 of model-simulated streamflow. *Journal of Geophysical Research: Atmo-*  
852 *spheres* 117, D03110.

853 Zeng, X., 2001. Global vegetation root distribution for land modeling. *Journal*  
854 *of Hydrometeorology* 2 (5), 525–530.